A Revised Approach to Ice Microphysical Processes for the Bulk Parameterization of Clouds and Precipitation

SONG-YOU HONG

Laboratory for Atmospheric Modeling Research, Department of Atmospheric Sciences, Yonsei University, Seoul, South Korea

JIMY DUDHIA

Mesoscale and Microscale Meteorology Division, National Center for Atmospheric Research, Boulder, Colorado

SHU-HUA CHEN

University of California, Davis, Davis, California

(Manuscript received 23 October 2002, in final form 7 July 2003)

ABSTRACT

A revised approach to cloud microphysical processes in a commonly used bulk microphysics parameterization and the importance of correctly representing properties of cloud ice are discussed. Several modifications are introduced to more realistically simulate some of the ice microphysical processes. In addition to the assumption that ice *nuclei* number concentration is a function of temperature, a new and separate assumption is developed in which ice *crystal* number concentration is a function of ice amount. Related changes in ice microphysics are introduced, and the impact of sedimentation of ice crystals is also investigated.

In an idealized thunderstorm simulation, the distribution of simulated clouds and precipitation is sensitive to the assumptions in microphysical processes, whereas the impact of the sedimentation of cloud ice is small. Overall, the modifications introduced to microphysical processes play a role in significantly reducing cloud ice and increasing snow at colder temperatures and slightly increasing cloud ice and decreasing snow at warmer temperatures. A mesoscale simulation experiment for a heavy rainfall case indicates that impact due to the inclusion of sedimentation of cloud ice is not negligible but is still smaller than that due to the microphysics changes. Together with the sedimentation of ice, the new microphysics reveals a significant improvement in high-cloud amount, surface precipitation, and large-scale mean temperature through a better representation of the ice cloud–radiation feedback.

1. Introduction

For the last two decades, cloud-resolving models (CRMs), also referred to as cumulus ensemble models (CEMs), have been applied to study convection and its interaction with a large-scale circulation (e.g., Soong and Tao 1980). CRMs employ the nonhydrostatic governing equations to resolve cloud-scale motions explicitly, with a horizontal grid spacing of less than a few kilometers. This approach uses state-of-the-art cloud models including sophisticated warm rain and ice schemes with several prognostic variables, for example, either mixing ratios (Lin et al. 1983; Rutledge and Hobbs 1983) or mixing ratios and number concentrations (Ferrier 1994), for various types of cloud and precipitation particles. CRMs have been recently applied to study tropical convection and its interaction between cloud-scale and large-scale circulations (Ferrier et al. 1995; Xu and Randall 1996; Tao et al. 1996; Grabowski 1998).

With the increase of computer power, it has become possible to implement sophisticated cloud and precipitation physics parameterizations developed within CRMs into general circulations models (GCMs) and numerical weather prediction (NWP) models. In the NWP and GCM areas, the portion of precipitation from a prognostic cloud and its precipitation processes is regarded as grid-resolvable precipitation, and subgrid-scale precipitation is due to parameterized cloud and precipitation processes from the cumulus parameterization scheme. In the mesoscale modeling area, the inclusion of prognostic cloud and precipitation schemes has improved quantitative precipitation simulation in large-scale forced situations, such as orographic or frontal ascent. In convective situations it is necessary to use such schemes in conjunction with a cumulus parame-

Corresponding author address: Song-You Hong, Dept. of Atmospheric Sciences, College of Science, Yonsei University, Seoul 120-749, South Korea.
E-mail: shong@yonsei.ac.kr

© 2004 American Meteorological Society

terization to avoid excessive grid-scale precipitation due to an unrealistic feedback between low-level heating, surface pressure fall, low-level moisture convergence, and upward motion (Zhang et al. 1988; Molinari and Dudek 1992). In the GCM community, the implementation of sophisticated microphysical processes for grid-resolvable precipitation physics is primarily used for realistic representation of the cloud–radiation feedback (Fowler et al. 1996; Ghan et al. 1997).

A bulk parameterization of cloud particles and precipitation drops that is primarily based on the works of Lin et al. (1983, hereafter LFO83) and Rutledge and Hobbs (1983, hereafter RH83), has been a core part of representing cloud and precipitation processes in both GCMs and mesoscale models. Dudhia (1989, hereafter D89) simplified the ice microphysical processes, designed for CRMs, for application in a mesoscale model, saving computational memory by not allowing mixed phase of ice and water. More recently, Grabowski (1998) took a similar approach to that of D89 in a CEM study for computational efficiency.

Although the double-moment approach of microphysics, predicting ice number concentrations as well as ice mixing ratios, (e.g., Ferrier 1994; Reisner et al. 1998) is promising, a diagnostic treatment of ice number concentrations has been used more in practice. Both LFO83 and RH83 diagnose ice number concentrations from cloud temperature using the relation from Fletcher (1962) without the effect of ice sedimentation. Modifications of their assumptions about the microphysical properties of ice clouds have been made in various newer schemes (e.g., Meyers et al. 1992; Krueger et al. 1995; Reisner et al. 1998; Rotstayn et al. 2000; Ryan 2000) that are based on observations or theoretical studies but also reflect that there is much uncertainty in this part of the parameterization schemes. Modifications include the definition of the number of ice crystals, the nucleation rate, and the size distribution of ice particles. An important reason for the modifications is to prevent too much ice in anvil and cirrus clouds so as to represent the cloud–radiation feedback realistically. For example, Meyers et al. (1992) proposed a relative-humidity-dependent ice number concentration contrasting with the temperature-only-dependent formula of Fletcher (1962), as is used in LFO83 and RH83. Krueger et al. (1995) revised the ice microphysics to include the Bergeron process. Reisner et al. (1998) adopted a snow-amount-dependent intercept parameter for snow and limited the ice number at colder temperatures to a fixed value. Rotstayn et al. (2000) and Ryan (2000) introduced a weakly temperature-dependent formula instead of Fletcher's. In addition to the improvement of microphysics, Manning and Davis (1997) pointed out the importance of the sedimentation of cloud ice from a statistical evaluation of real-time forecasts. Wang (2001) also pointed out the importance of ice sedimentation in simulating tropical cyclone structure.

This study addresses the issue of cloud microphysical properties in a commonly used bulk cloud parameterization scheme and investigates the importance of microphysical parameters in simulating cloud-scale to mesoscale convective systems. Some modifications of microphysical properties are introduced to D89 and RH83 to more realistically represent the ice microphysical processes. Realizing the uncertainty in the definition of ice number concentrations and its subsequent effects in ice processes, we propose a new ice microphysics where cloud ice number concentration is diagnosed from its mixing ratio. Section 2 describes the microphysical processes of clouds and precipitation. In section 3, the modified assumptions in the schemes will be tested for an idealized thunderstorm case, and their impact will further be investigated in a 3D forecast setup for a heavy rainfall event that occurred over the Korean peninsula. The paper concludes with a discussion of other sensitivity experiments conducted and relevant modifications of microphysical processes made in previous studies.

2. Modifications of microphysical processes introduced to a commonly used bulk cloud scheme

The bulk cloud microphysics algorithms adopted in this study are based on D89 and RH83, which are implemented in the National Centers for Environmental Prediction (NCEP) regional spectral model (Hong et al. 1998). The two schemes with modifications explained below are being implemented in the Weather Research and Forecasting (WRF) model (Klemp et al. 2000; Michalakes et al. 2001; Chen and Dudhia 2000), as the NCEP simple ice (three classes: vapor, cloud/ice, and rain/snow) and mixed phase (five classes: vapor, cloud, ice, rain, and snow) schemes. Hong et al. (1998) examined the importance of the complexity of microphysical properties on mesoscale forecasts. They concluded that the simple ice scheme without mixed-phase microphysics is enough to resolve mesoscale features on a 25-km grid. Dudhia's (1989) approach predicts three categories of moisture: vapor, cloud water/ice, and rain/snow. The cloud ice and cloud water are counted as the same category, and they are distinguished by temperature. That is, the category is considered to be cloud ice when the temperature is less than or equal to the freezing point, otherwise it is considered to be cloud water. This scheme is computationally efficient with realistic representation of ice physics on a 10–30-km model grid, giving results comparable to a mixed-phase scheme having five categories of moisture in which supercooled water and melting snow are additionally allowed to exist. Modifications of microphysics introduced in this study are based on recent observations and physical consistency of the cloud microphysical properties, which will presently be described. Major modifications since RH83 and D89 include a temperature-dependent intercept parameter for snow, cloud-ice-mass-dependent ice number concentration and related

changes in ice processes, autoconversion of cloud water to rain, and the inclusion of sedimentation of ice crystals. The sensitivity of simulated precipitation systems to the changes will be presented in section 3. All units in this section are in MKS.

a. Sedimentation of falling ice crystals

Based on the observational evidence for gravitational sedimentation of ice crystals, we adopted the mean terminal velocity of falling ice proposed by Heymsfield and Donner (1990, hereafter HD90), which can be expressed by

$$\overline{V}_I \text{ (m s}^{-1}) = 3.29(\rho q_I)^{0.16}, \quad (1)$$

where ρ is air density and q_I is the mixing ratio of cloud ice. Ice crystals then fall into environments for removal through sublimation, accretion, and autoconversion. The sedimentation velocities in (1) are 0.5, 0.7, and 1.0 m s^{-1} for q_I equal to 0.01×10^{-3}, 0.1×10^{-3}, and 1.0×10^{-3} kg kg^{-1}, respectively. New velocity–diameter formulas were developed by Heymsfield and Iaquinta (2000, hereafter HI2000). Using the aspect ratio information from balloon-borne ice crystal replicator data, they developed theoretical terminal velocities for bullet rosettes, single bullets, and columns as a function of maximum dimension (D_I), which can be expressed with their masses by

$$V_I = xD_I^{\gamma}, \qquad M_I = \alpha D_I^{\beta}, \quad (2)$$

where x, y, α, β are coefficients depending on the habit of ice crystals. The formula (2) requires the information about the ice number concentration in order to be used practically in a bulk model. As will be shown below, we merged the two formulas, (1) and (2), by formulating a new ice number concentration function that is consistent with both.

b. Ice mass, diameter, and number concentration relationship

Most existing bulk cloud microphysics schemes adopt the formula of Fletcher (1962) for the number concentration of ice nuclei, which is based on standard ice nucleus measuring techniques and is given by

$$N_I \text{ (m}^{-3}) = 10^{-2} \exp[0.6(T_0 - T)], \quad (3)$$

where T is temperature and T_0 is the freezing point (273.15 K). This formula produces a concentration increase of a factor of 10 for about every 4°C cooling. The computed values are bounded by an upper value, for example, 10^9 m^{-3} in the scheme used in the fifth-generation Pennsylvania State University–National Center for Atmospheric Research Mesoscale Model (MM5), version 3 (Grell et al. 1994). Fletcher's formula does not have a theoretical basis for clouds of temperature less than −35°C. However, many cirrus in midlatitudes have a cloud-top temperature below −50°C, and Fletcher's formula has been criticized for producing too many small ice crystals in the upper troposphere (Meyers et al. 1992; Manning and Davis 1997). In this situation, a large part of the cloud ice is not removed from the upper troposphere, but is carried in extensive, long-lived cloud shields. To resolve this deficiency, other formulations have been proposed for N_I that include other dependent variables in addition to temperature. For example, Meyers et al. (1992) proposed N_I with a function of relative humidity. Rotstayn et al. (2000) modified the Meyers's formula with a supersaturation-dependent expression.

We believe it is important to distinguish between the number concentration of ice *nuclei*, as formulated by Fletcher (1962), for instance, and the activated ice *crystal* number concentration that depends not only upon the local availability of ice nuclei but also on the history of the air parcel carrying the ice crystals. Two-moment schemes predict number concentration as an independent variable and can therefore incorporate such information directly, but we chose to continue with a one-moment scheme. Double-moment schemes such as Ferrier (1994) and Reisner et al. (1998) are beyond the scope of this study and often have complex numerical issues associated with separately advecting mass and number concentration fields. More recent observations [than Fletcher (1962)] reported in Ryan (2000) show that the relation between ice crystal number concentration and cloud temperature is not consistent from case to case [see Fig. 5 of Ryan (2000)], but there are measurements from several field programs that show a correlation between ice mass and number concentration (A. Heymsfield 2002, personal communication). The ice mass is affected by processes including ice initiation, deposition, sublimation, accretion, autoconversion, advection, and sedimentation. By relating number concentration to ice mass these processes also indirectly affect number concentration, which is realistic and addresses a perceived deficiency in one-moment schemes that parameterize number concentration solely in terms of local thermodynamic variables.

In this study, we derive the N_I as a function of cloud ice mixing ratio by assuming that the HD90 sedimentation, a function of ice mixing ratio, is consistent with individual crystal fall speeds given by HI2000, as this puts a desired constraint on the number of crystals. Combining the fall velocity of ice in (1) and (2), by using the mean mass of an ice crystal ($M_I = \rho q_I / N_I$) together with a mass–diameter relation, N_I can be expressed as

$$N_I \text{ (m}^{-3}) = c(\rho q_I)^d, \quad (4)$$

where c and d are coefficients depending on the ice crystal habit. For single column, single bullet, and rosettes, c is 3.02×10^7, 5.38×10^7, and 2.76×10^8, and d is 0.72, 0.75, and 0.80, respectively (Heymsfield and Iaquinta 2000). For rosettes, we use three component bullets as a typical value. Figure 1 shows the re-

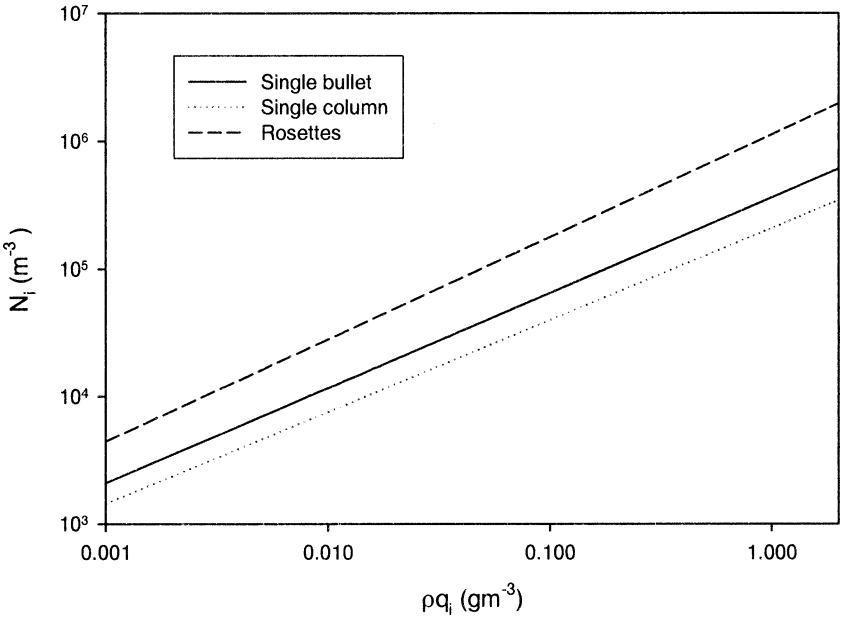

FIG. 1. Ice crystal numbers as a function of cloud ice amount derived in this study.

lation of N_I with cloud ice mixing ratio that seems to give a reasonable variation of N_I with ice mass. Given the typical range of q_I, N_I ranges from 10^4 to 10^5 m^{-3}. This range of N_I complies with the recent observational analyses for N_I (Ryan 2000). At a given cloud ice amount, N_I gets larger in turn for single columns, bullets, and rosettes, but the relative difference is not significant. In a preliminary test, it was found that the choice of the habit of ice in N_I does not result in a significant impact on microphysical behavior. Thus, we chose the median set of values N_I, which is that for single bullets.

The resulting mass, diameter, and number concentration relationships developed in this study are as follows:

$$V_I \text{ (m s}^{-1}) = 1.49 \times 10^4 D_I^{1.31}, \quad (5a)$$

$$D_I \text{ (m)} = 11.9 M_I^{0.5}, \quad (5b)$$

$$N_I \text{ (m}^{-3}) = 5.38 \times 10^7 (\rho q_I)^{0.75}, \quad (5c)$$

$$\rho q_I \text{ (kg m}^{-3}) = 4.92 \times 10^{-11} N_I^{1.33},$$
$$= 8.38 \times 10^{30} M_I^4,$$
$$= 2.08 \times 10^{22} D_I^8, \quad (5d)$$

where again all units are in MKS. We slightly changed the coefficients for the mass–diameter relation for simplicity. The mass versus diameter formula has a square power as in RH83. Recall that Eq. (5c) ensures that the mean terminal velocity, $\overline{V}_I$, is the same as that of Heymsfield and Donner (1990) [Eq. (1)] for a given cloud ice amount when this relation is used in conjunction with a velocity–diameter relation (5a) derived by Heymsfield and Iaquinta (2000). The current scheme allows for consistent ice crystal sizes to be used for both sedimentation and ice microphysical processes, which is an improved aspect compared to the old scheme. Existing schemes implicitly ignore this connection unless they relate the fall speed of ice crystals to a mean diameter that is also used in the microphysics.

c. Intercept parameter for snow (n_{0S})

RH83 and D89 treat the spectral intercept parameter for snow (n_{0S}) as a constant (2×10^7 m^{-4}) despite its strong dependency on temperature in nature (Ryan 1996). Based on Houze et al. (1979), n_{0S} can be expressed as

$$n_{0S} \text{ (m}^{-4}) = 2 \times 10^6 \exp[0.12(T_0 - T)]. \quad (6)$$

The above formula indicates an increase of the n_{0S} as the temperature decreases. The computed values are given an upper bound of 2×10^8 m^{-4} since there is no observational evidence at cloud temperatures below -35°C (Ryan 1996). With this formula, the slope parameter of the size distributions for snow, $\lambda_S = (\pi \rho_S n_{0S}/\rho q_S)^{1/4}$, where ρ_S is the density of snow and q_S is the mixing ratio of snow, increases from 10^3 m^{-1} to 10^4 m^{-1} as cloud temperature decreases for typical snow concentrations of 0.1×10^{-3} to 1×10^{-3} kg kg^{-1}. This formula implicitly represents broadening of the snow spectra at higher temperature that is well documented in observational studies (Houze et al. 1979; Ryan 1996).

The value of 2×10^7 m^{-4} of RH83 and D89 corresponds to that at $T = -19.5$°C in Eq. (6). The increase of n_{0S} at colder temperatures means an increase of snow number concentration, which enhances the rate of accretion of ice and sublimation/deposition of snow and reduces the sedimentation of snow through the reduced mean size of snow aggregates.

d. Initiation of cloud ice crystal (Pgen)

For RH83 and D89, the initiation rate of cloud ice from water vapor when $T < 0$°C and the air is supersaturated with respect to ice under the no ice condition was given by

$$\text{Pgen}\,(\text{kg kg}^{-1}\,\text{s}^{-1}) = \min[(q_{I0} - q_I)/\Delta t, (q - q_{SI})/\Delta t], \quad (7)$$

where Pgen ≥ 0, Δt is the time step, q is the water vapor mixing ratio, q_{SI} is its saturated value with respect to ice, q_{I0} is $M_{I0}N_{I0}/\rho$, and M_{I0} is the initial mass of cloud ice that corresponds to 10^{-12} kg. It can be seen that given the N_{I0} of Fletcher (1962), $N_{I0}M_{I0}/\rho$ is usually greater than q_I in the upper troposphere, which leads to a bounded value of Pgen at $(q - q_{SI})/\Delta t$. For example, $M_{I0}N_{I0}/\rho$ is 0.1×10^{-3} kg kg^{-1} for $T = -38.5$°C, and 1.0×10^{-3} kg kg^{-1} for $T = -42.5$°C. For temperatures below -43°C, Pgen assumes the supersaturated amount of water vapor with respect to ice, and all the supersaturation is removed immediately.

In this study, we treat the ice crystal number concentration (N_I) separately from the ice nuclei number concentration (N_{I0}). Here, N_I is diagnosed from Eq. (5c), while N_{I0} is diagnosed from Eq. (8). This differs from the MM5 and RH83/D89 methodology that used Eq. (3) for diagnosing both N_I and N_{I0}. The number of ice nuclei is assumed to be greater at colder temperatures, but not as sensitive to temperature as Fletcher's (1962) formula, and can be expressed by

$$N_{I0}(\text{m}^{-3}) = 10^3 \exp[0.1(T_0 - T)]. \quad (8)$$

Cloud ice mixing ratio, q_{I0}, then can be diagnosed from Eq. (5d) to be consistent with the mass–number relation (Fig. 2b). Thus the ice nuclei number determines the maximum ice crystal mass that can be initiated given sufficient ice supersaturation, and both N_{I0} and ρq_{I0} increase with decreasing temperature. Note that the Reisner scheme in the MM5 has a limit for ρq_{I0} to prevent unrealistic ice generation processes. We keep the formula of Eq. (7) as in LFO83 and D89, but N_{I0} ranges from 10^3 to 10^5 m^{-3}, relative to extreme values from Fletcher's formula. Equation (8) gives $N_{I0} = 1 \times 10^4$ m^{-3}, $\rho q_{I0} = 0.01 \times 10^{-3}$ kg m^{-3} at -23°C, and $N_{I0} = 1 \times 10^5$ m^{-3}, $\rho q_{I0} = 0.2 \times 10^{-3}$ kg m^{-3} at -46°C. Figure 2b shows that the new scheme initiates more cloud ice at temperatures warmer than -38°C, whereas initiation of cloud ice is almost not allowed at these temperatures by the Fletcher formula. The new scheme no longer uses the concept of an initial ice crystal mass M_{I0}, but instead uses Eq. (5d) to maintain consistency between total ice mass and number concentration with this initiation process.

e. Vapor deposition of a small ice crystal (Pisd)

For RH83 and D89, the growth rate of ice crystals by deposition of water vapor, when the air is supersaturated with respect to ice, was given by using the mean mass of an ice crystal ($M_I = \rho q_I/N_I$) and the mass–diameter relation in Eq. (5b),

$$\text{Pisd}\,(\text{kg kg}^{-1}\,\text{s}^{-1}) = \frac{4\overline{D}_I(S_I - 1)N_I}{A_I + B_I} = \frac{4\overline{D}_{\text{Icon}}(S_I - 1)(\rho q_I N_I)^{0.5}}{A_I + B_I}, \quad (9)$$

where S_I is the ice saturation (q_{SI}/q), A_I and B_I are thermodynamic functions (see, e.g., D89). Here, $\overline{D}_{\text{Icon}}$ is 11.9 instead of 16.3, used by RH83 and D89. Because of the new formulation of N_I that generally implies larger crystals, Pisd is slower at colder temperatures, as it should be, whereas Pisd was unrealistically active at colder temperatures in RH83 (Fig. 3). Our formula for Pgen is more active at colder temperatures than Pisd, which

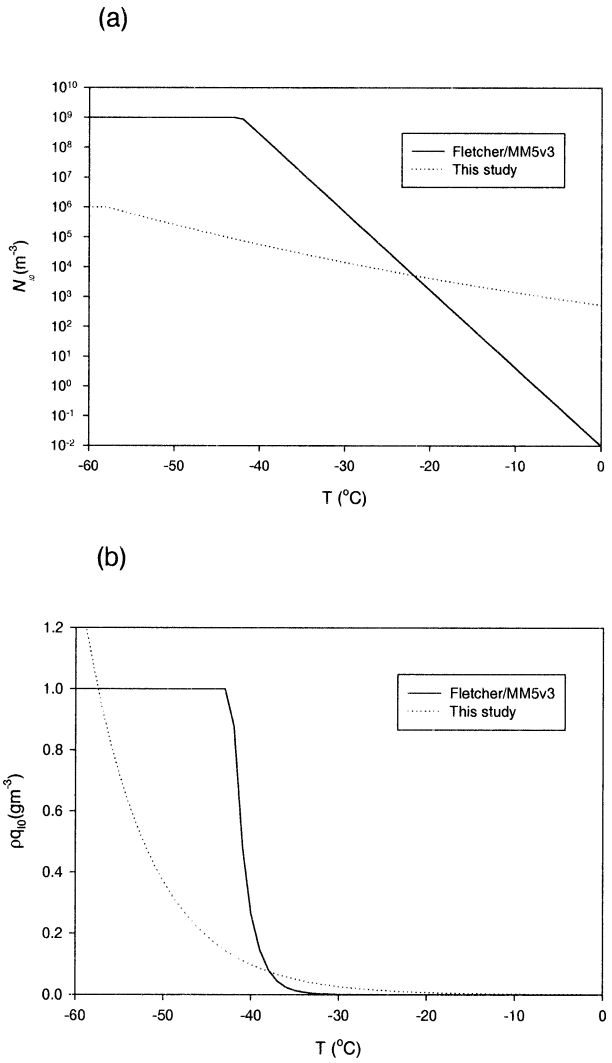

FIG. 2. (a) Ice nuclei number concentration in Eq. (8) and (b) initial ice crystal amount for generation as a function of temperature from the Fletcher (1962) scheme in MM5 and derived in this study.

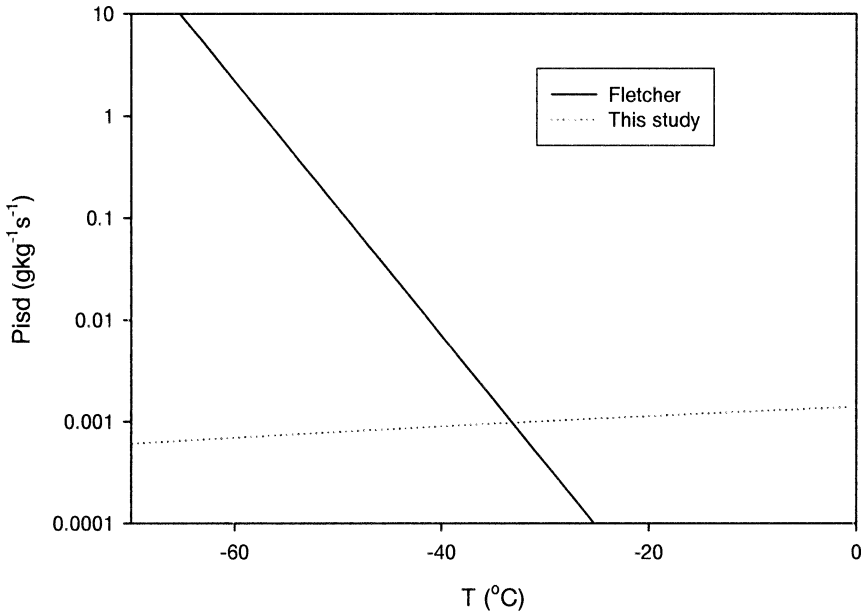

FIG. 3. Comparison of deposition rate of water vapor onto ice as a function of cloud temperature, with the assumption that cloud ice mixing ratio is 0.1 g kg^{-1} and the air is supersaturated with respect to ice by 10%.

is more active at warmer temperatures. The formulation Pgen is responsible for the initiation of small ice crystals in favorable conditions where few or none existed before while the further growth of crystals is taken into account by the deposition process, but this also has an implicit initiation because of the mass–number relation that is assumed to always hold. For RH83, both processes are more active at cold temperatures because of the use of higher number concentrations implying smaller crystals.

f. Accretion of cloud ice by snow (Pacr)

The accretion rate of cloud ice by snow is parameterized as in RH83 and D89 and is given by

$$\text{Pacr (kg kg}^{-1}\text{ s}^{-1}) = \frac{\pi a_S q_I E_{\text{SI}} n_{0S}}{4}\left(\frac{\rho_0}{\rho}\right)^{1/2}\frac{\Gamma(b_S+3)}{\lambda_S^{b_S+3}}, \quad (10)$$

in which the accretion efficiency, E_{SI}, is a constant at 0.1, $b_S = 0.41$ is the exponent, and $a_S = 11.72$ is the multiplier in the snowfall-speed formula. Note that as in LFO83 and D89, Eq. (10) was derived without considering the effect of cloud ice sedimentation. The effect of ice sedimentation in the accretion of cloud ice by snow can be adopted in the future (M. Gilmore 2003, personal communication). Based on physical justification, accretion of cloud ice by snow is more active at higher temperature (LFO83), so a new efficiency function is expressed by

$$E_{\text{SI}} = \exp[0.05(T - T_0)], \quad (11)$$

where T_0 is the freezing temperature (273.15K). The formula in (11) is similar to a temperature-dependent efficiency in LFO83 but has a more rapid decrease of the efficiency at colder temperatures. On the other hand, an opposing effect at colder temperatures is expected because of the increase of n_{0S} in (6).

g. Conversion of ice crystals to snow (Paut$_I$)

For RH83, the autoconversion (aggregation) rate of ice crystals to snow was given by

$$\text{Paut (kg kg}^{-1}\text{ s}^{-1}) = \max[(q_I - q_{\text{Icrit}})/\Delta t, 0], \quad (12)$$

where q_{Icrit} ($M_{\text{Imax}}N_I/\rho$) is the threshold value for autoconversion of ice crystals and M_{Imax} represents the maximum allowed ice crystal mass. As in the formula of ice generation, q_{Icrit} has a small range of temperatures between $-27°$ and $-32°$C for typical ice particles of 0.1×10^{-3} to 1.0×10^{-3} kg kg^{-1}. In other words, existing ice crystals are converted to snow when the temperature is warmer than $-27°$C and has nearly no chance for conversion when $T < -32°$C. This is due to the rapid exponential increase of N_I in the Fletcher (1962) formula as the temperature decreases, as seen in Fig. 2a.

We keep the same value for the maximum diameter of ice ($D_{\text{Imax}} = 500$ μm) for autoconversion as in RH83 and D89 and this provides the critical mixing ratio of ice from the relation given by Eq. (5d) as

$$q_{\text{Icrit}} \text{ (kg kg}^{-1}) = 8 \times 10^{-5}/\rho. \quad (13)$$

Equation (13) does not have a strong temperature de-

pendency as in the RH83 and D89, but autoconversion is slightly suppressed at colder temperatures because of the effect of density of air. At $T = -40$°C and $P = 300$ hPa, q_{Icrit} becomes 0.18×10^{-3} kg kg^{-1}.

h. Sublimation and depositional growth of snow/ evaporation of rain (Pres)

The evaporation of rainwater is calculated if the air is subsaturated with respect to water, and the formula [Eq. (B14) in D89] is very similar to that for snow sublimation given below. For snow, however, the formula is with respect to ice saturation, where both subsaturation and supersaturation may occur. As in RH83 and D89, the continuous growth equation is given by

$$\text{Pres (kg kg}^{-1}\text{ s}^{-1}) = \frac{4n_{0S}(S_I - 1)}{(A_I + B_I)} \times \left\{ \frac{0.65}{\lambda_S^2} + 0.44 S_c^{1/3} \left(\frac{a_S \rho}{\mu} \right)^{1/2} \left(\frac{\rho_0}{\rho} \right)^{1/4} \times \frac{\Gamma[(b_S + 5)/2]}{\lambda_S^{(b_S+5)/2}} \right\}, \quad (14)$$

where S_c is the Schmidt parameter and μ is the dynamic viscosity of air. Compared to the process with $n_{0S} = 2 \times 10^7$ m^{-4} in RH83 and D89, the formula for n_{0S} in this study (6) produces larger (smaller) Pres at colder (warmer) temperatures, consistent with the assumed broadening of the snow size spectrum.

i. Autoconversion of cloud water to rain (Paut$_C$)

Autoconversion is the process whereby cloud droplets form raindrops through collisions with each other. Following Kessler (1969), the autoconversion rate of cloud water to rain may be written as

$$\text{Paut (kg kg}^{-1}\text{ s}^{-1}) = \alpha(q_C - q_{C0}), \quad (15)$$

in which the autoconversion rate from cloud water, q_C, to rain depends on a critical liquid water content for cloud water (q_{C0}). Here an autoconversion parameterization with a stronger physical basis (Tripoli and Cotton 1980, hereafter TC80) is adopted and can be expressed by

$$\text{Paut (kg kg}^{-1}\text{ s}^{-1}) = -\frac{0.104 g E_c \rho^{4/3}}{\mu (N_C \rho_w)^{1/3}} q_C^{7/3} H(q_C - q_{C0}), \quad (16)$$

where μ is the dynamic viscosity of air (1.718×10^{-5} kg m^{-1} s^{-1}), ρ_w is the density of water, N_C is the droplet concentration (3×10^8 m^{-3}), g is the acceleration due to gravity, E_c is the mean collection efficiency (0.55). Also, $H(x)$ is the Heaviside unit step function, which suppresses the autoconversion processes until cloud water reaches a critical mixing ratio (q_{C0}),

$$q_{C0}\text{ (kg kg}^{-1}) = \frac{4\pi \rho_w r_{\text{cr}}^3 N_C}{\rho}, \quad (17)$$

where r_{cr} is the critical mean droplet radius at which the autoconversion begins.

The formula of TC80 is more physically based than Kessler's (1969). It can be shown that the TC80 scheme represents a similar conversion rate to that of Kessler for q_C less than 1×10^{-3} kg kg^{-1} and a faster conversion for larger droplets. However, for typical values of q_C less than 1×10^{-3} kg kg^{-1}, the two formulas convert the cloud droplets similarly despite the complexity in TC80. As pointed out by LFO83, the critical mixing ratio is important in the Kessler formula. This value has been tuned to a smaller value of 0.5×10^{-3} or 0.7×10^{-3} kg kg^{-1}, relative to the original value of 1×10^{-3} kg kg^{-1} in LFO83 to produce raindrops realistically on a mesoscale grid. Likewise, r_{cr} is an important parameter in the TC80 formula. We set the value to 8 μm instead of 10 μm used in TC80. With a value of 10 μm, the threshold value for conversion is 1.28×10^{-3} kg kg^{-1}, which is similar to the threshold used in the LFO83. In addition, the TC80 formula is consistent with the autoconversion of ice to snow in Eqs. (12)–(13) through the introduction of number concentration of cloud droplets. The number concentration of cloud droplets is also a tunable parameter that may be larger in unpolluted and marine environments.

3. Numerical experiments

Modifications in the microphysics of clouds and precipitation are implemented in the WRF model as the ''NCEP cloud 3'' and ''NCEP cloud 5'' schemes. The WRF model is a community model suitable for both research and forecasting (Chen and Dudhia 2000; Klemp et al. 2000; Michalakes et al. 2001; Chen and Sun 2002). This model is well suited for idealized types of simulations to study baroclinic waves, idealized storm dynamics, or topographically induced flows, as well as for detailed NWP cases with real-data initial states and boundary conditions. The version of the model used is 1.2.1, released in May 2002.

Two sets of experiments are carried out: an idealized 2D thunderstorm case and a 3D real-data simulation of a heavy rainfall event. The idealized thunderstorm experiment is designed to systematically distinguish the intrinsic differences between the RH83 and D89 microphysics and the revised ice processes described in section 2 by the virtue of fixed initial conditions and lack of other nonmicrophysical processes, which in turn will help us to understand the impact of the changes in microphysics in the 3D framework. For both 2D and 3D experiments, a simple ice microphysics (NCEP cloud 3) is selected for grid-resolvable precipitation physics. In the idealized experiments, other physical processes are turned off, whereas they are included for the heavy rainfall simulation. The Kain–Fritsch (1993) cumulus parameterization scheme is selected to account for subgrid-scale precipitation processes. A nonlocal vertical diffusion scheme is used to calculate the vertical fluxes

TABLE 1. A key to the microphysics schemes.

Code	Description
Exp1	RH83 and D89 microphysics
Exp2	RH83 and D89 microphysics plus sedimentation of ice crystals
Exp3	Modified microphysics described in section 2
Exp4	Modified microphysics described in section 2 plus sedimentation of ice crystals
PLS	Purdue Lin (Chen and Sun 2002) microphysics

of sensible heat, latent heat, and momentum (Hong and Pan 1996). A simple shortwave radiation scheme is used (Dudhia 1989), and a multiband longwave radiation package is selected (Mlawer et al. 1997).

Four experiments are carried out for each case (Table 1). Experiment 1 (Exp1) employs the same microphysical processes as in D89 and RH83 (i.e., not the modified processes described in section 2). Since the impact of sedimentation of ice turned out to be significant, experiments are designed to separately account for the sedimentation of ice and other microphysical processes. Experiment 2 (Exp2) includes the sedimentation of ice but not the new microphysics. Experiment 3 (Exp3) incorporates the modifications of microphysical processes described in section 2, excluding the sedimentation of ice particles. Experiment 4 (Exp4) considers all modifications proposed in this study. A fifth experiment (PLS) uses the three-class ice parameterization, which is called a ''Purdue Lin scheme'' in the WRF model (Chen and Sun 2002). The Purdue Lin microphysics scheme is based on Lin et al. (1983) and Rutledge and Hobbs (1984), with some modifications. This scheme in WRF is similar to the version in Chen and Sun (2002) except for considering sedimentation of cloud ice. We show the results with the Purdue Lin scheme just as a reference run since microphysics in RH83, D89, and Chen and Sun (2002) are different in many respects. Major discussion will be focused on the comparison of Exp1–Exp4 with the simple ice run since the impact of modifications in microphysics commonly appears in both simple and mixed-phase schemes. The sedimentation formula for ice crystals in Exp2 and Exp4 follows that proposed by HD90. Note that sedimentation formula with the new ice physics is the same for both HD90 and HI2000, whereas the HI2000 individual crystal fall speeds do not apply when the old ice microphysics is employed (Exp2).

a. Idealized thunderstorm experiment

The idealized thunderstorm simulation is a present option for the WRF model. We chose a 2D domain in the x direction. The grid in the x direction is 201 points with a 250-m grid spacing. The number of vertical layers is 80. The model is integrated for 60 min with a time step of 3 s. The initial condition has a warm bubble that has a radius of 4 km and a maximum perturbation of 3 K at the center of the domain. A 12 m s^{-1} wind is applied in the positive x direction at the surface, decreasing to zero at 2.5 km above the ground, with no wind above. Open boundary conditions are applied, and there is no Coriolis force or friction. The only physical parameterization is the microphysical scheme. This experiment serves to show the behavior of the microphysics in a quasi-steady setting that simplifies the interpretation of the results. After an hour simulation, the thunderstorm started to move in the x direction within the periodic lateral boundaries.

Figure 4 compares the condensate fields from Exp4 to those from the PLS experiment. The PLS experiment is referred to as a reference run since it predicts cloud water, cloud ice, snow, graupel, and rainwater explicitly. Despite the simplified representation of ice processes in Exp4, the scheme shows its capability of simulating fundamental features of a well-organized thunderstorm. The general structure of the thunderstorm, such as the cloud/ice water in the updraft region near the storm center and anvil clouds, is well simulated. Cloud condensate reaches a maximum in the middle troposphere in the area of the updraft for both experiments. A wider area of the rain shaft in the PLS experiment may be due to higher fall speed of precipitation due to the inclusion of graupel. The overall resemblance of the results from the cloud 3 and Purdue Lin schemes assures us that the simplified ice microphysical processes are reasonable for even this high resolution of 250 m in the horizontal. The basic features of the simulated storm are unchanged from Exp1 to Exp4, but the detailed structure is different, as shown below.

Figure 5 compares profiles of domain-averaged condensate and precipitation mixing ratios for Exp1–Exp4. Overall, the impact of sedimentation of falling ice is small without considering our modifications of microphysics since the use of Fletcher's (1962) formula for diagnosing both N_{I0} and N_I allows too many small ice crystals to be generated and persist in the upper troposphere, and these do not grow into snow crystals at a significant rate. Only a slight reduction of q_I in the anvil centered at the 10-km level is visible (Fig. 5; cf. Exp1 and Exp2). It is apparent that the distribution of cloud ice is more uniform in the vertical through the incorporation of ice microphysics introduced in this study (cf. Exp1 and Exp3). The average cloud content at upper levels is decreased by more than a factor of 2. An increase of ice is also distinct in the lower part of the ice clouds below 8 km. The ice crystal mixing ratio in the anvil ranges from 0.1×10^{-3} to 1×10^{-3} kg kg^{-1} in Exp1, whereas the range is from 0.01×10^{-3}

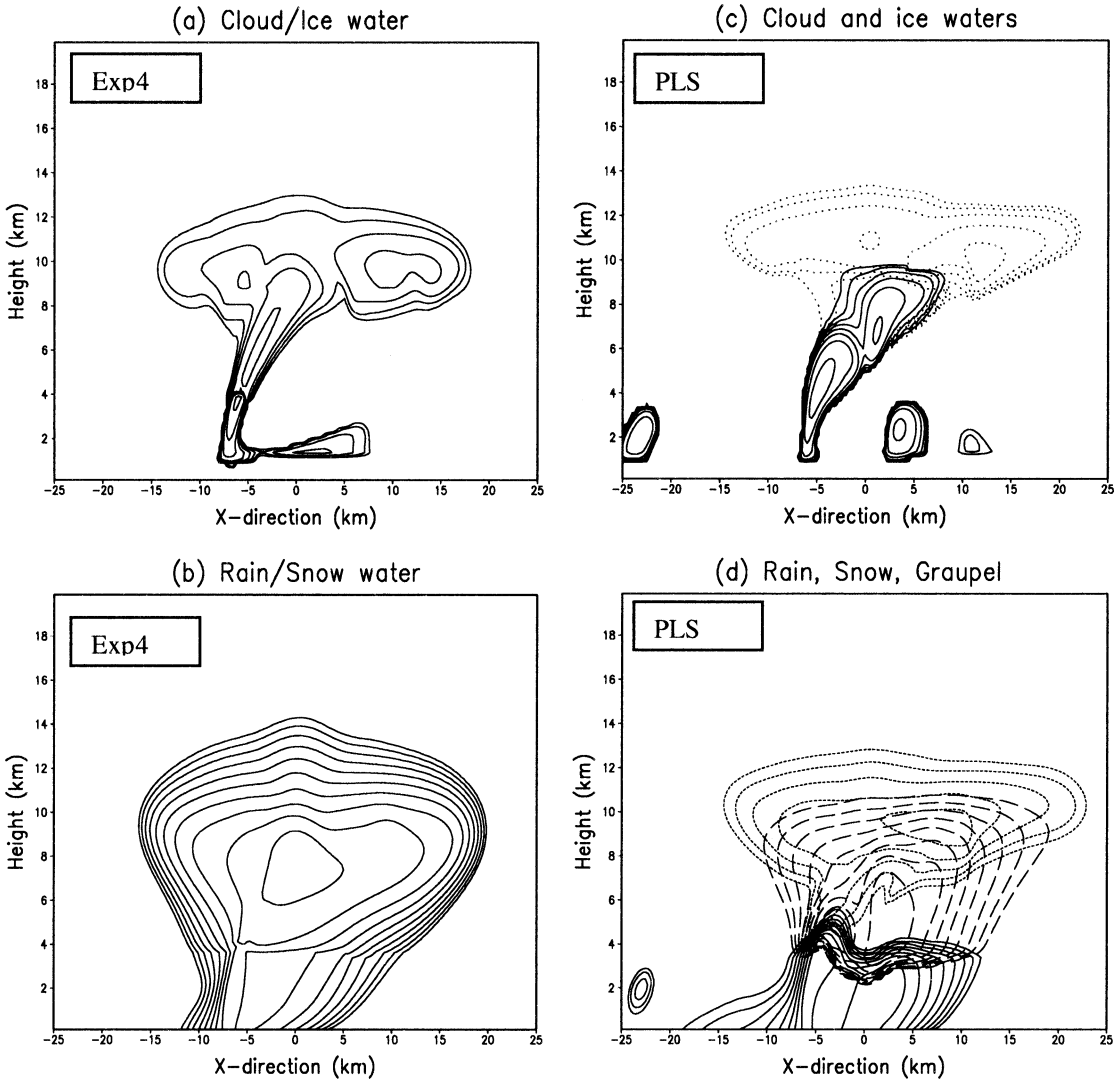

FIG. 4. Isolines of the condensate fields for (a) cloud/ice water and (b) rain/snow water from Exp4, and (c) ice (dotted) and cloud (solid) water and (d) snow (short dashed), graupel (long dashed), and rain water (solid) mixing ratios from the PLS experiment after a 60-min integration. Contour lines are at 0.01, 0.02, 0.04, 0.08, 0.16, 0.32, 0.64, 1.28, 2.56, 5.12, and 10.24 g kg^{-1}.

to 0.1×10^{-3} kg kg^{-1} in Exp3. This smaller magnitude of q_I in Exp3 is closer to some observations in cold cloud ice shields (HI2000). As compensation, there is an increase of snow at the colder temperatures and a decrease at warmer temperatures.

The distribution characteristics of ice and snow are a combined effect of the modifications in the ice microphysics described in section 2. The reduction of ice and the increase of snow at colder temperatures are due mostly to the increase of n_{0S} and non-temperature-dependent ice number concentration. The increase of n_{0S} at colder temperatures enhances the rate of accretion of ice and sublimation/deposition of snow. The new formulas for ice nucleation [Eqs. (7)–(8)] also reduce (increase) the initial generation of ice at temperatures cooler than -38°C (warmer than -38°C) when ice does not exist. The rate of ice deposition (9) is also decreased because of smaller ice number concentrations at colder temperatures but is more active at warmer temperatures. Accretion of ice particles onto snow (10)–(11) is active at midcloud layers, together with the effect of n_{0S}. The conversion process from ice to snow (12) is less active at warmer temperatures and more active at colder temperatures (see Fig. 2). The reduction of cloud water below 4 km is found to be due to an indirect impact of ice microphysics rather than the change of autoconversion following TC80. The effect of the inclusion of ice sedimentation is still small compared to the changes in microphysics but more distinct when the new microphysics is employed (cf. Exp3 and Exp4). The introduction of sedimentation of ice particles reduces the ice amount in the upper part of ice shields but does not affect the snow distribution.

Modifications in the ice microphysical processes re-

duce the ice crystals and increase the snow at colder temperatures and does alleviate a discontinuity of ice and snow distributions seen in vertical soundings by also increasing the ice and decreasing the snow at warmer temperatures.

b. Heavy rainfall case experiment

A heavy rainfall event is selected in this study to investigate the impact of the new parameterization on the simulated precipitation and upper-atmospheric large-scale properties. A significant amount of precipitation was recorded in Korea on 25 July 1997 (Fig. 6), with a local maximum of about 170 mm in the west-central part of South Korea and another of about 90 mm at the southeastern flank of the peninsula. Most of the rainfall was observed during the 12-h period from 0000 to 1200 UTC 25 June 1997. Before the onset of heavy precipitation at 0000 UTC 25 June, moderate rain was observed at the southwestern part of Korea, with less than 40 mm between 1200 UTC 24 June and 0000 UTC 25 June 1997. Associated with the heavy rainfall over Korea, there was a low pressure system centered over the Yellow Sea, with a warm front to the east and a cold front to the southwest, that was embedded within a monsoon circulation (Fig. 7a). Associated with this low pressure system, convective activity is visible both to the south of the cold front and to the north of the warm front (Fig. 7b).

From the upper-level analyses (not shown), it is found that a southerly low-level jet (LLJ), which was associated with a cyclonic circulation centered over the low system and an anticyclonic circulation along the western flank of a subtropical high, brought moisture northward. As the low pressure system moved northeastward and the subtropical high further extended to the west, the LLJ south of a monsoon front was intensified. The enhanced LLJ brought moisture to the Korean peninsula. The upper-level circulation shows intensification of a thermal ridge over the peninsula and a trough to the west of the surface low system centered over the Yellow Sea. These LLJ and upper-level patterns satisfy the synoptic circulation favorable for developing heavy precipitation over the Korean peninsula (Lee et al. 1998; Chen et al. 1999).

Initial and boundary conditions are based on the global analysis and prediction system that is routinely produced operationally at NCEP. Incorporating information from upper-level sounding data through the MM5 analysis system further enhances initial conditions, and these files are then adapted for input to the WRF system using the MM52WRF converter program. The 48-h experiments start at 1200 UTC 23 June 1997, 36 h prior to the onset of heavy precipitation in the Korean peninsula. The model is run at 45-km grid spacing in the horizontal on a Lambert-conformal conic projection with 23 levels in the vertical. The number of horizontal grid points in both x and y directions is 80, centered on the Korean peninsula covering the area of Fig. 7a. A higher-resolution experimental setup is desired, but the current version of the WRF model does not have a nesting capability. The PLS experiment will only briefly be discussed in the final section since this graupel scheme was not designed for such large grid sizes.

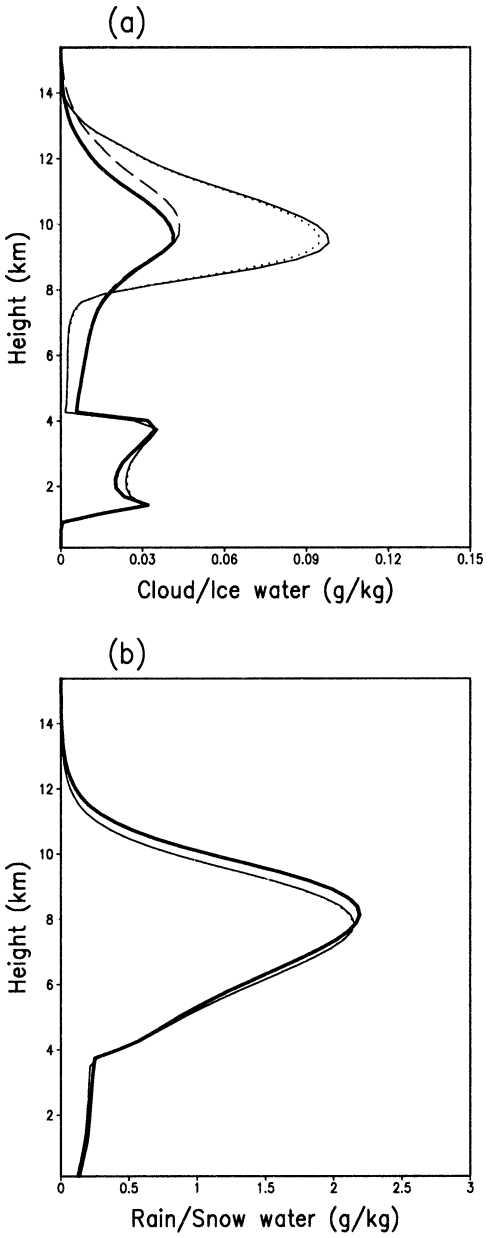

FIG. 5. Profiles of domain-averaged (a) cloud/ice water and (b) snow/rain water mixing ratio (g kg^{-1}) for Exp1 (thin solid line), Exp2 (dotted line), Exp3 (dashed line), and Exp4 (thick solid line).

Table 2 shows the statistics of simulated precipitation over South Korea and the domain-averaged 300-hPa temperature. The number of surface observation stations over South Korea is 72, which is about 35-km horizontal resolution. The 24-h accumulated observed precipitation

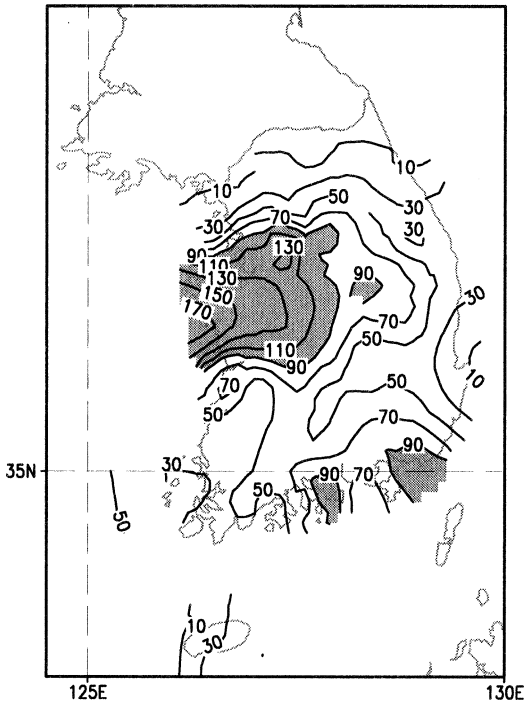

FIG. 6. The 24-h accumulated precipitation (mm), valid at 1200 UTC 25 Jun 1997, over the Korean peninsula.

data are linearly interpolated on the WRF grid by using a simple objective analysis (Cressman 1959) to compute the statistics. The spatial pattern correlation coefficient is computed between simulated and observed precipitation on the WRF grids for each experiment. The bias score for precipitation for each experiment is the ratio of the area-averaged simulated precipitation over the observed value. The 300-hPa temperature is verified over the NCEP reanalysis that is used to provide the lateral boundary data. The bias and rms values averaged over the model domain are the difference and root-mean-square error values between simulation and reanalysis, respectively.

TABLE 2. The pattern correlation and bias score of 24-h accumulated precipitation over South Korea, ending at 1200 UTC 25 Jun 1997, and the bias and root-mean-square error of 300-mb temperature over the whole domain, valid at 0000 UTC 25 Jun 1997, resulting from the simple ice (mixed phase) experiments.

	Precipitation		300-mb *T*	
	Correlation	Bias score	Bias (K)	Rms (K)
Exp1	0.41 (0.47)	0.53 (0.63)	1.24 (1.32)	1.55 (1.61)
Exp2	0.43 (0.48)	0.58 (0.65)	1.11 (1.20)	1.42 (1.49)
Exp3	0.47 (0.50)	0.58 (0.64)	1.07 (1.13)	1.36 (1.41)
Exp4	0.64 (0.70)	0.67 (0.68)	0.16 (0.19)	0.84 (0.87)
PLS	0.50	0.73	0.58	1.06

It is clear that Exp4 improves the precipitation scores over Korea by enhancing the precipitation activity in both cloud 3 and cloud 5 schemes. Meanwhile, the improvement of the 300-hPa mean temperature is distinct in Exp4. The improvement of precipitation scores by enhanced precipitation and reduced warm bias in Exp4 are not only due to the improvement of microphysics, but are also due to a better cloud–radiation feedback, which is an indirect effect of the new scheme and which will further be discussed at the end of this section.

Overall, the impact of the microphysics for the heavy rainfall case follows the scenario revealed in the idealized experiments but with a larger impact in the upper part of cloud shields because of the incorporation of a radiation feedback in the 3D model framework (Fig. 8). The impact of the changes in microphysics and the ice sedimentation on simulated ice clouds follows the characteristics analyzed in the idealized experiments (Fig. 8a) but with sedimentation having more impact possibly because of the longer time scale of this simulation. For example, the decrease of ice in the upper part of clouds

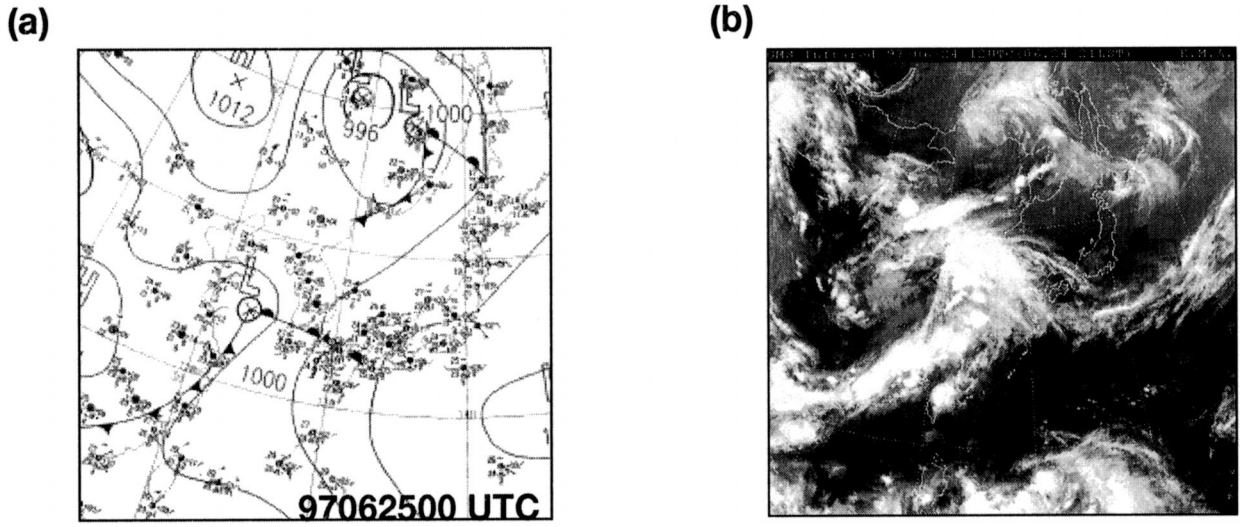

FIG. 7. (a) Surface analyses and (b) satellite image at 0000 UTC 25 Jun 1997.

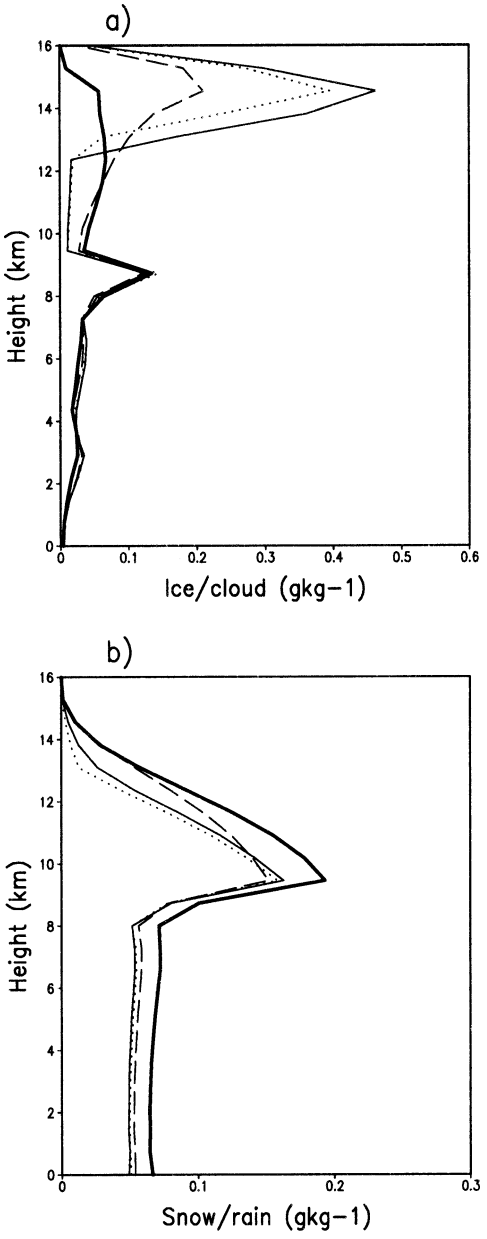

FIG. 8. Vertical profiles of (a) the ice/cloud water mixing ratios and snow/rain water mixing ratios averaged over Korea (33°–40°N, 122°–130°E) at 0000 UTC 25 Jun 1997, obtained from Exp1 (thin solid), Exp2 (dotted), Exp3 (dashed), and Exp4 (thick solid).

is distinct in going from Exp1 to Exp2 and from Exp3 to Exp4. The increase of ice at warmer temperatures is pronounced, as in the idealized experiments. The monotonic decrease of the sum of ice and snow in Exp4 with decreasing temperature is consistent with the results from Ryan (2000). The combined effect of improved microphysics and sedimentation of ice provides a significant effect on the cloud and precipitation particles. In Exp3 and Exp4, coexisting ice and snow are seen at warmer temperatures below 13 km, whereas there is negligible ice at these levels in Exp1 and Exp2. On the other hand, the sensitivity of the distribution of snow/rain is different from the behavior revealed in the idealized experiments. The impact of the changes in the microphysics alone on the snow/rain distribution follows that in the idealized case above $z = 4$ km. However, unlike in the idealized case, the addition of sedimentation also has a significant impact, considerably increasing the snow/rain within the entire troposphere below 13 km.

Both schemes relate sedimentation to ice mass by HD90 (Exp2 and Exp4), but Fig. 8 shows that there is a stronger effect when sedimentation of ice is added to the new microphysics. This is mostly due to an enhanced conversion to snow when sedimentation is activated, while the former scheme's snow amount is unaffected by adding sedimentation (Exp2). This happens because when the ice mass is reduced at a high level by sedimentation the new scheme (Exp4) also reduces the number of ice crystals through (4), while the old scheme, where the number is only a function of temperature following Fletcher [1962; Eq. (3)] would unrealistically assume the same number to be distributed in the smaller remaining mass. Hence sedimentation in the new scheme leads to fewer crystals that still easily convert to faster falling snow, thereby enhancing the fallout, while the old scheme implies many smaller crystals that cannot convert, and thus the slower HD90 sedimentation rate continues to apply.

In Fig. 9, the 24-h accumulated precipitation amounts during the heavy precipitation period from Exp1 and Exp4 are shown. The resulting point values of accumulated precipitation, due to the changes of microphysics and inclusion of sedimentation, are increased by 20 mm over Korea. The enhanced precipitation seen in Exp4 is closer to what was observed (Table 2), owing to better areal coverage of the heavy rain. However, we note that many more case studies are needed to determine whether the improvements in Exp4 give forecasts that are consistently closer to the observed rainfall. An increase of precipitation was evident in Exp2 and Exp3 over Korea but was much smaller than that from Exp4. Note that the increased portion of precipitation over Korea is mostly due to the grid-resolvable precipitation physics. The convective parameterization scheme is responsible for less than 2 mm of the accumulated precipitation (not shown) during the 24-h period of precipitation in Fig. 9. This is due to that fact that heavy rainfall over Korea is linked with a nearly saturated atmospheric structure up to the middle troposphere embedded in the east Asian summer monsoon front (Hong and Lee 1994; Lee et al. 1998; Chen et al. 1999). It is interesting to note that major features of simulated precipitation remain unchanged by the introduction of the new physical processes and the inclusion of sedimentation of cloud ice (Fig. 9), despite some improvement of precipitation forecast skill scores (Table 2). The distribution of simulated precipitation was similar to that in Exp4 when the Purdue Lin scheme is introduced (not

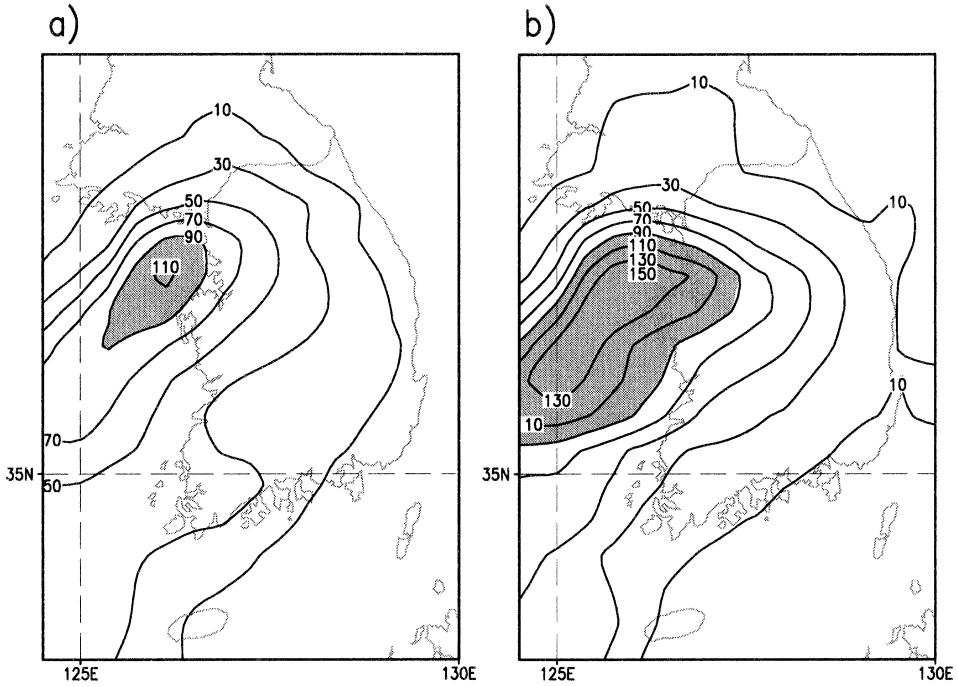

FIG. 9. The 24-h accumulated precipitation (mm) valid at 1200 UTC 25 Jun 1997, obtained from (a) Exp1 and (b) Exp4.

shown). This implies that the heavy rainfall case selected in this study is synoptically organized, as is typical for heavy rainfall in Korea (Lee et al. 1998).

The time evolution of domain-averaged precipitation amounts due to subgrid-scale (implicit) processes from the convective parameterization scheme and the grid-resolvable (explicit) processes from the cloud microphysics is shown in Fig. 10. Note that most of the precipitation over Korea in Fig. 9 is due to microphysics, as explained in the previous paragraph. Most of the implicit rain in Fig. 10 appears in southern China, where convective instability is a key mechanism (not shown). Consistent with the sensitivity of precipitation mixing ratio in Fig. 8, the increase of surface rain is pronounced in Exp4, particularly during the heavy precipitation period over Korea from the 30- to 48-h forecast time. The domain-total implicit rain experiences a distinct diurnal variation because of the nature of the Kain–Fritsch convective parameterization. Enhanced convective activity is found during the late afternoon in Exp4, which is an indirect effect of the microphysical process on large-scale features. This issue will be further addressed at the end of this section.

In Fig. 11, we show the vertically integrated ice/cloud water mixing ratio at 0000 UTC 25 June 1997. In the figure, rain/snow is identified over the precipitation areas in southern China, Korea, and northern Manchuria (not shown). It is apparent that too much cloud condensate is simulated in Exp1 when the modifications in section 2 are not considered (cf. Figs. 11a and 7b). Large amounts of cloud over the ocean south of Japan are spurious. As stated in the discussion of Fig. 8, the microphysics plays a more significant role than the sedimentation of ice in reducing the spurious ice in the upper atmosphere. For example, the spurious ice shields over the oceans south of Japan still exist in Exp3, with a smaller amount than in Exp1 and Exp2 (not shown).

The amount of cloud ice/water keeps increasing with time, being greatest in Exp1, followed by Exp2 and Exp3, while Exp4, with the new scheme, shows the slowest increase after the initial adjustment for a few hours (Fig. 12a). This monotonic increase of cloudiness with time in Exp1–Exp3 was reported in the previous literature. Manning and Davis (1997) showed such an increase of clouds when the sedimentation of ice particles is not considered, whereas Hong et al. (1998) demonstrated that the same trend was observed when a diagnostic precipitation process is employed or when horizontal advection of clouds is not considered. The improvement in large-scale mean temperature is striking (Fig. 12b). Exp4 is capable of suppressing the synoptic-scale drift of the simulated large-scale temperature. Compared to the sensitivity of cloudiness, the impact of either sedimentation of ice or microphysics only is much smaller than the combined effect. The same improvement was obtained for moisture fields by suppressing the monotonic increase of moisture with time. The correction of the large-scale bias is also found below 400 hPa, but with a smaller magnitude than in the upper troposphere.

Additional experiments were conducted to reveal the cause of the 300-hPa warm bias in Exp1. The NORA,

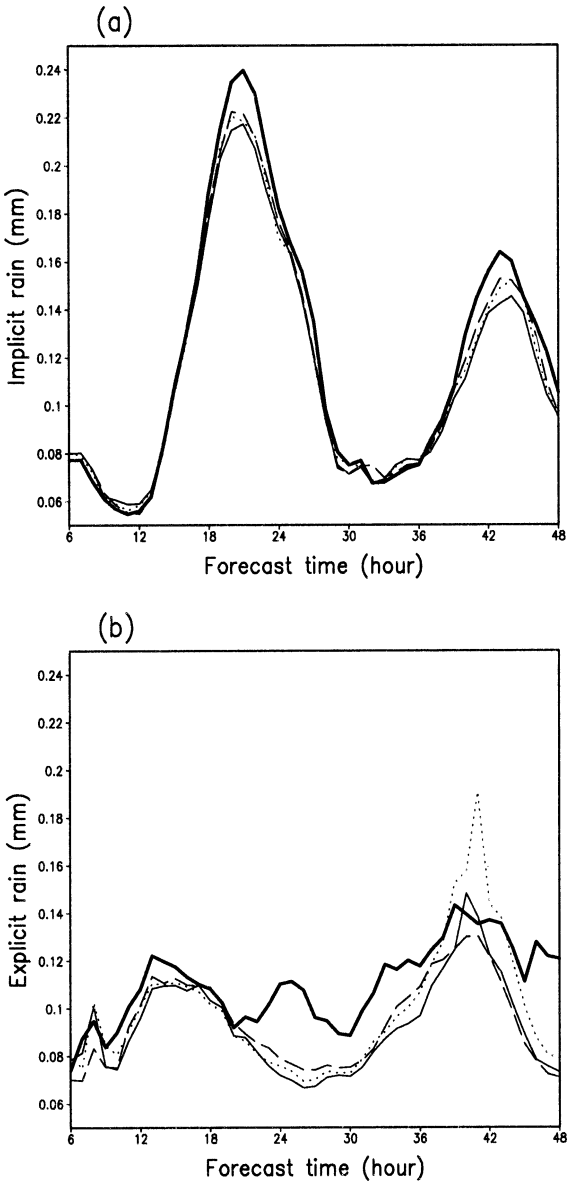

FIG. 10. Model domain-averaged 1-h accumulated (a) subgrid-scale (implicit) rain and (b) grid-resolvable (explicit) rain, obtained from Exp1 (thin solid), Exp2 (dotted), Exp3 (dashed), and Exp4 (thick solid).

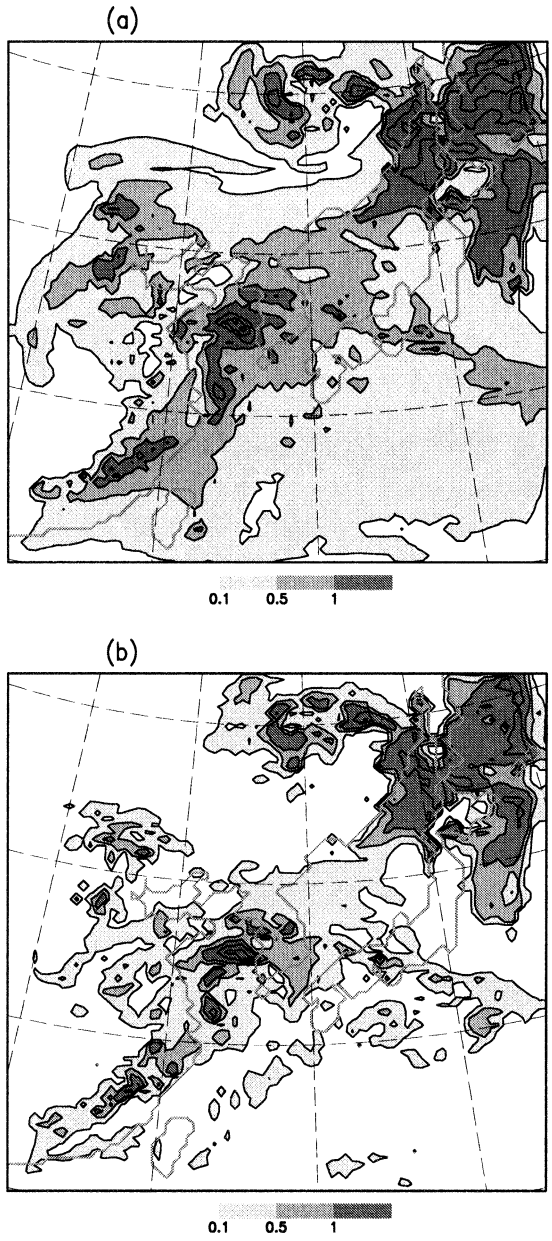

FIG. 11. Vertically integrated cloud/ice water (g m^{-3}) for (a) Exp1 and (b) Exp4 at the 36-h forecast, which is valid at 0000 UTC 25 Jun 1997.

NOLW, and NOSW experiments are the same as Exp1 but exclude the radiative effects of short- and longwave heating due to ice particles. In other words, the NORA, NOLW, and NOSW experiments exclude *both* short and longwave heating, *longwave* heating, and *shortwave* heating due to ice, respectively. From Fig. 13, it can be seen that, while the effect on cloud amount is quite small, the removal of longwave–cloud interaction cools the troposphere below the cirrus, while the removal of shortwave–cloud interaction has a warming effect there. It can be inferred that excessive longwave radiation heating, due to trapping by too much ice cloud above, is the cause of the warm bias in Exp1. A reduction of shortwave heating in the troposphere due to cirrus shading is an opposite effect to that from the longwave, but has a much smaller impact. The absence of the ice cloud–radiation interaction increases surface precipitation (Table 3); this means that more (less) ice cloud decreases (increases) surface precipitation (Fig. 13a). Note again that precipitation over Korea is mostly due to explicit microphysics, whereas most of the implicit (convective) rain is simulated in southern China. It is evident that neglecting the shortwave–ice cloud inter-

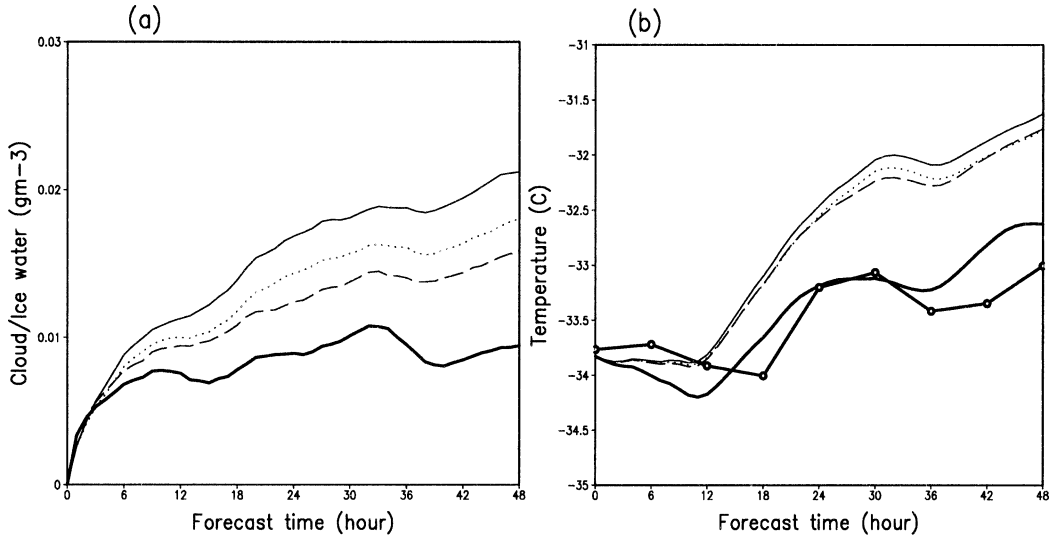

FIG. 12. Time variation of (a) volume-averaged cloud/ice water (g m^{-3}) and (b) domain-averaged temperature at 300 hPa, obtained from Exp1 (thin solid), Exp2 (dotted), Exp3 (dashed), and Exp4 (thick solid) and the analyses (solid line with open circles).

action affects the amount of implicit rain due to parameterized convection, whereas the longwave radiation influences the explicit rain due to microphysical processes significantly. Having more implicit rain in the NOSW experiment is found to be due to the fact that more shortwave heating near the surface increases the moist static energy, which in turn leads to an increase in the convective available potential energy. Meanwhile, more explicit rain in the NOLW experiment is likely due to the fact that a colder temperature in the absence of longwave–ice cloud interaction increases the relative humidity in the upper troposphere.

4. Concluding remarks

This study discusses the importance both of cloud microphysical processes in a commonly used bulk microphysics parameterization and of the sedimentation of cloud ice. A modified version of the microphysics is evaluated for an idealized 2D thunderstorm and for a heavy rainfall case over east Asia within the WRF model framework. Several modifications are introduced to more realistically simulate some of the ice microphysical processes. Major modifications from RH83 and D89 include 1) the Houze et al. (1979) temperature-depen-

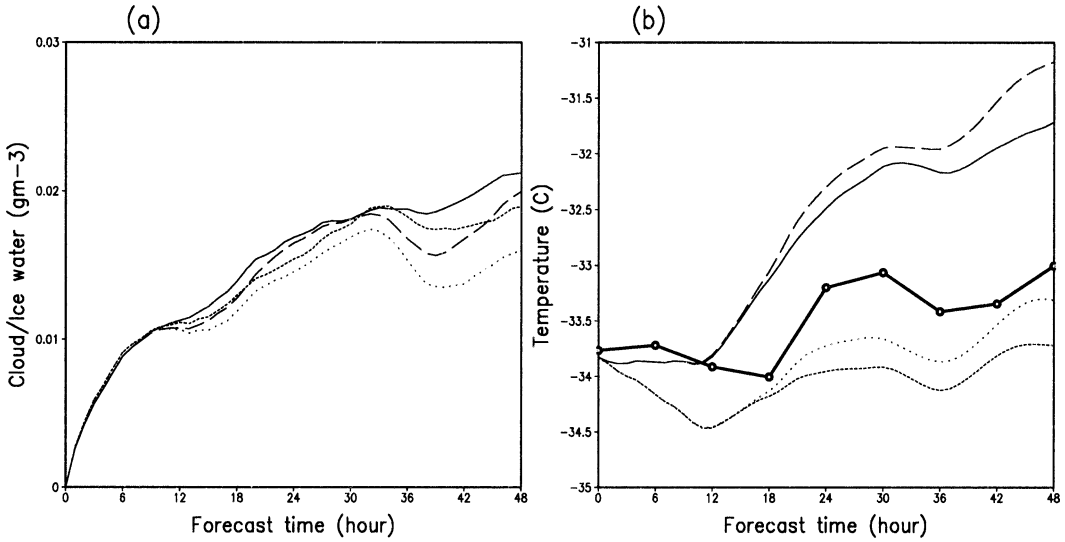

FIG. 13. Same as Fig. 12, but for the Exp1 (thin solid), NORA (dotted), NOLW (short dashed), and NOSW (long dashed) experiments.

TABLE 3. The model domain-averaged 48-h accumulated precipitation (mm).

Experiment	Implicit rain	Explicit rain	Total
Exp1	5.30	4.19	9.49
NORA	6.23	4.95	11.18
NOLW	5.53	4.40	9.93
NOSW	6.15	4.45	10.61

dent intercept parameter for snow, 2) a new formula for diagnosing cloud ice number concentration from cloud ice mass, 3) a modified formula for diagnosing cloud ice nucleation and 4) related changes in ice processes, 5) autoconversion of cloud water to rain following TC80, and 6) the inclusion of the sedimentation of falling ice crystals. Modifications in the ice microphysical processes result in a realistic distribution of clouds by reducing the ice crystals and by increasing the snow at colder temperatures, and by removing the discontinuity of ice and snow in the vertical profiles. Autoconversion of cloud water to rain proposed by TC80 is very similar to Kessler's (1969) formula, with an appropriate setting of the radius of cloud droplets.

In an idealized thunderstorm simulation, the distributions of simulated clouds and precipitation are sensitive to the assumptions in microphysical processes, whereas the impact of the sedimentation of cloud ice is relatively small. The introduction of the changes in microphysics reduces anvil ice by a factor of 2 and increases snow at warmer temperatures. The model was able to reproduce cloud structures similar to a more sophisticated graupel scheme (Chen and Sun 2002). Gilmore et al. (2002) have also confirmed the importance of microphysical parameters in high-resolution grids.

In the heavy rainfall experiments, a combined effect of microphysics and sedimentation of ice provides an improvement of cloud shield area, upper-tropospheric mean temperature, and surface precipitation, whereas either the microphysics or the sedimentation alone is not enough to remove the spurious cloud extent. The new ice microphysics allows less cloud ice to persist at colder temperatures by allowing the number concentration to implicitly decline as the ice mass is depleted by sedimentation and autoconversion. The main reason for the improvement of surface precipitation and 300-hPa mean temperature in the new scheme was found to be due to a better representation of ice cloud properties affecting the cloud–radiation feedback. Ice cloud affects the longwave heating more significantly than the shortwave heating in terms of upper-level mean temperature. Shortwave–ice cloud interaction affects the amount of parameterized convection, whereas the longwave radiation influences the microphysical (explicit) rain.

Historically, mesoscale models such as MM4 (Anthes and Warner 1978) did not include a radiation–atmosphere feedback but have included a sophisticated warm-rain microphysics (Hsie et al. 1984), whereas the radiation for the ground energy budget was represented in a column-integrated manner. Zhang et al. (1988) formulated a mesoscale model system also without a cloud–radiation feedback to successfully simulate the evolution of a mesoscale precipitation system. After the inclusion of ice microphysics and a cloud–radiation feedback in MM5 (Dudhia 1989), reduction was seen in an upper-level relative humidity bias, and some important effects of the melting level below stratiform anvils were simulated (e.g., Zhang 1992). However, a cool daytime bias at the surface began to appear in some cases (Dudhia 1996), which was associated with too much cirrus from previous convection in multiday simulations, and this was substantially improved by adding sedimentation following the formula of HD90 into the D89 cloud microphysics. Manning and Davis (1997) showed that the inclusion of ice sedimentation also improved the model high-cloud cover. Ghan et al. (1997) and Grabowski (1998) demonstrated that the treatment of microphysical processes is very important for the interaction between convection and the large-scale environment. Our results help to confirm that both increased sophistication in the microphysics and the sedimentation of cloud ice need to be taken into account in cloud-scale, mesoscale, and general circulation models.

Finally, the performance of the scheme varies from one case to another. In contrast to a similar performance of the new scheme with the Purdue Lin scheme for the present case, the new scheme outperforms the Purdue Lin scheme irrespective of the choice of the cumulus parameterization scheme for a heavy rainfall case over the United States (Kain et al. 2002), but there is a need for more case studies and verification to more fully determine the effectiveness of this new scheme.

The NCEP cloud 3 and cloud 5 schemes available in WRF version 1.1 already had modifications to D89 and RH83, including the temperature-dependent snow intercept parameter, the temperature-dependent LFO83 ice accretion efficiency, and the TC80 cloud autoconversion formula, while version 1.2 added the HD90 ice sedimentation process. The changes described in this paper, mostly related to ice number concentration and ice initiation, will be implemented in future versions of these schemes in WRF.

Acknowledgments. The authors would like to express their gratitude to the Korea Meteorological Administration (KMA) for providing the satellite images and observed precipitation analyses. This study is supported by the Ministry of Science and Technology through the National Research Laboratory Program, KOSEF through the SRC Program, and by KMA through the R&D Project. A part of this work has been done during the first author's (SYH) visit to NCAR, which was supported partly by NCAR. We are grateful to Tae-Young Lee, John Brown, and Joe Klemp for their interest and encouragement. Jeong-Ock Lim helped to revise the code, which should be acknowledged. Thanks go also

to Kevin Manning, Bill Hall, Matthew Gilmore, and an anonymous reviewer for helpful suggestions on the manuscript.

REFERENCES

Anthes, R. A., and T. T. Warner, 1978: Development of hydrodynamic models suitable for air pollution and other mesometeorological studies. *Mon. Wea. Rev.*, **106,** 1045–1078.

Chen, S.-H., and J. Dudhia, cited 2000: Annual report: WRF physics. [Available online at http://www.mmm.ucar.edu/wrf/users/wrf_phy.html.]

——, and W.-Y. Sun, 2002: A one-dimensional time dependent cloud model. *J. Meteor. Soc. Japan,* **80,** 99–118.

Chen, S.-J., D.-K. Lee, Z.-Y. Tao, and Y.-H. Kuo, 1999: Mesoscale convective system over the Yellow Sea—A numerical case study. *Meteor. Atmos. Phys.*, **70,** 185–199.

Cressman, G. P., 1959: An operational objective analysis system. *Mon. Wea. Rev.*, **87,** 367–374.

Dudhia, J., 1989: Numerical study of convection observed during the winter monsoon experiment using a mesoscale two-dimensional model. *J. Atmos. Sci.*, **46,** 3077–3107.

——, 1996: Data assimilation of a ten-day period during June 1993 over the Southern Great Plains Site using a nested mesoscale model. Preprints, *Seventh Conf. on Mesoscale Processes*, Reading, United Kingdom, Amer. Meteor. Soc., 416–417.

Ferrier, B. S., 1994: A double-moment multiple-phase four-class bulk ice scheme. Part I: Description. *J. Atmos. Sci.*, **51,** 249–280.

——, W.-K. Tao, and J. Simpson, 1995: A double-moment multiple-phase four-class bulk ice scheme. Part II: Simulations of convective storms in different large-scale environments and comparisons with other bulk parameterizations. *J. Atmos. Sci.*, **52,** 1001–1033.

Fletcher, N. H., 1962: *The Physics of Rain Clouds.* Cambridge University Press, 390 pp.

Fowler, L. D., D. A. Randall, and S. A. Rutledge, 1996: Liquid and ice cloud microphysics in the CSU General Circulation Model. Part I: Model description and simulated microphysical processes. *J. Climate,* **9,** 489–529.

Ghan, S. J., R. Leung, and Q. Hu, 1997: Application of cloud microphysics to NCAR community climate model. *J. Geophys. Res.*, **102** (D14), 16 507–16 527.

Gilmore, M. S., J. M. Straka, and E. N. Rasmussen, 2002: Quantitative precipitation in simulated deep convection: Sensitivity to the hail/graupel category. Preprints, *15th Conf. on Numerical Weather Prediction,* San Antonio, TX, Amer. Meteor. Soc., 139–142.

Grabowski, W. W., 1998: Toward cloud resolving modeling of large-scale tropical circulations: A simple cloud microphysics parameterization. *J. Atmos. Sci.*, **55,** 3283–3298.

Grell, G. A., J. Dudhia, and D. Stauffer, 1994: A description of the fifth-generation Penn State/NCAR Mesoscale Model (MM5). NCAR Tech. Note NCAR/TN-398+STR, 117 pp.

Heymsfield, A. J., and L. J. Donner, 1990: A scheme for parameterizing ice cloud water content in general circulation models. *J. Atmos. Sci.*, **47,** 1865–1877.

——, and J. Iaquinta, 2000: Cirrus crystal terminal velocities. *J. Atmos. Sci.*, **57,** 916–938.

Hong, S.-Y., and D.-K. Lee, 1994: Numerical simulation of a meso-β scale heavy rainfall event over the Korean peninsula. Preprints, *10th Conf. on Numerical Weather Prediction*, Portland, OR, Amer. Meteor. Soc., 245–247.

——, and H.-L. Pan, 1996: Nonlocal boundary layer vertical diffusion in a medium-range forecast model. *Mon. Wea. Rev.*, **124,** 2322–2339.

——, H.-M. H. Juang, and Q. Zhao, 1998: Implementation of prognostic cloud scheme for a regional spectral model. *Mon. Wea. Rev.*, **126,** 2621–2639.

Houze, R. A., P. V. Hobbs, P. H. Herzegh, and D. B. Parsons, 1979: Size distributions of precipitation particles in frontal clouds. *J. Atmos. Sci.*, **36,** 156–162.

Hsie, E.-Y., R. A. Anthes, and D. Keyser, 1984: Numerical simulation of frontogenesis in a moist atmosphere. *J. Atmos. Sci.*, **41,** 2581–2594.

Kain, J., and M. Fritsch, 1993: Convective parameterization for mesoscale models: The Kain–Fritsch scheme. *The Representation of Cumulus Convection in Numerical Models, Meteor. Monogr.*, No. 24, Amer. Meteor. Soc., 165–170.

——, M. Baldwin, and S. Weiss, 2002: WRF model evaluation at the SPC and NSSL. Preprints, *15th Conf. on Numerical Weather Prediction,* San Antonio, TX, Amer. Meteor. Soc., 256–259.

Kessler, E., 1969: *On the Distribution and Continuity of Water Substance in Atmospheric Circulations. Meteor. Monogr.,* No. 32, Amer. Meteor. Soc., 84 pp.

Klemp, J. B., W. C. Skamarock, and J. Dudhia, cited 2000: Conservative split-explicit time integration methods for the compressible nonhydrostatic equations. [Available online at http://www.mmm.ucar.edu/wrf/users/wrf-dyn-num.html.]

Krueger, S. K., Q. Fu, and K. N. Kiou, 1995: Improvements of an ice-phase microphysics parameterization for use in numerical simulations of tropical convection. *J. Appl. Meteor.*, **34,** 281–287.

Lee, D.-K., H. R. Kim, and S.-Y. Hong, 1998: Heavy rainfall over Korea during 1980–1990. *Korean J. Atmos. Sci.*, **1,** 32–50.

Lin, Y.-L., R. D. Farley, and H. D. Orville, 1983: Bulk parameterization of the snow field in a cloud model. *J. Appl. Meteor.*, **22,** 1065–1092.

Manning, K. W., and C. A. Davis, 1997: Verification and sensitivity experiments for the WISP94 MM5 forecasts. *Wea. Forecasting,* **12,** 719–735.

Meyers, M. P., P. J. DeMott, and W. R. Cotton, 1992: New primary ice-nucleation parameterization in an explicit cloud model. *J. Appl. Meteor.*, **31,** 708–721.

Michalakes, J., S. Chen, J. Dudhia, L. Hart, J. Klemp, J. Middlecoff, and W. Skamarock, 2001: Development of a next-generation regional weather research and forecast model. *Developments in Teracomputing,* W. Zwieflhafer and N. Kreitz, Eds., World Scientific, 269–296.

Mlawer, E. J., S. J. Taubman, P. D. Brown, M. J. Iacono, and S. A. Clough, 1997: Radiative transfer for inhomogeneous atmosphere: RRTM, a validated correlated-k model for the long wave. *J. Geophys. Res.*, **102** (D14), 16 663–16 682.

Molinari, J., and M. Dudek, 1992: Parameterization of convective precipitation in mesoscale numerical models: A critical review. *Mon. Wea. Rev.*, **120,** 326–344.

Reisner, J., R. M. Rasmussen, and R. T. Bruintjes, 1998: Explicit forecasting of supercooled liquid water in winter storms using the MM5 mesoscale model. *Quart. J. Roy. Meteor. Soc.*, **124,** 1071–1107.

Rotstayn, L. D., B. F. Ryan, and J. J. Katzfey, 2000: A scheme for calculation of the liquid fraction in mixed-phase stratiform clouds in large-scale models. *Mon. Wea. Rev.*, **128,** 1070–1088.

Rutledge, S. A., and P. V. Hobbs, 1983: The mesoscale and microscale structure and organization of clouds and precipitation in midlatitude cyclones. Part VIII: A model for the ''seeder-feeder'' process in warm-frontal rainbands. *J. Atmos. Sci.*, **40,** 1185–1206.

——, and ——, 1984: The mesoscale and microscale structure and organization of clouds and precipitation in midlatitude cyclones. Part XII: A diagnostic modeling study of precipitation development in narrow cloud-frontal rainbands. *J. Atmos. Sci.*, **41,** 2949–2972.

Ryan, B. F., 1996: On the global variation of precipitating layer clouds. *Bull. Amer. Meteor. Soc.*, **77,** 53–70.

——, 2000: A bulk parameterization of the ice particle size distribution and the optical properties in ice clouds. *J. Atmos. Sci.*, **57,** 1436–1451.

Soong, S.-T., and W.-K. Tao, 1980: Response of deep tropical cumulus clouds to mesoscale processes. *J. Atmos. Sci.*, **37,** 2016–2034.

Tao, W.-K., S. Lang, J. Simpson, C.-H. Sui, B. Ferrier, and M.-D. Chou, 1996: Mechanisms of cloud–radiation interaction in the Tropics and midlatitudes. *J. Atmos. Sci.,* **53,** 2624–2651.

Tripoli, G. J., and W. R. Cotton, 1980: A numerical investigation of several factors contributing to the observed variable intensity of deep convection over south Florida. *J. Appl. Meteor.,* **19,** 1037–1063.

Wang, Y., 2001: An explicit simulation of tropical cyclones with a triply nested movable mesh primitive equation model: TCM3. Part I: Model description and control experiment. *Mon. Wea. Rev.,* **129,** 1370–1394.

Xu, K.-M., and D. A. Randall, 1996: Explicit simulation of cumulus ensembles with the GATE Phase III data: Comparison with observations. *J. Atmos. Sci.,* **53,** 3710–3736.

Zhang, D.-L., 1992: The formation of a cooling-induced mesovortex in the trailing stratiform region of a midlatitude squall line. *Mon. Wea. Rev.,* **120,** 2763–2785.

——, E.-Y. Hsie, and M. W. Moncrieff, 1988: A comparison of explicit and implicit predictions of convective and stratiform precipitating weather systems with a meso-β-scale numerical model. *Quart. J. Roy. Meteor. Soc.,* **114,** 31–60.